ChemComm

Impacts of oxo interactions within actinyl metal organic materials: Highlight on thermal expansion behaviour

Journal:	*ChemComm*
Manuscript ID	CC-COM-06-2018-005240.R1
Article Type:	Communication

Journal Name

COMMUNICATION

Impacts of oxo interactions within actinyl metal organic materials: Highlight on thermal expansion behaviour

Maurice K. Payne, Mikaela M. Pyrch, Matthew Jubinsky, Madeline C. Basile, and Tori Z. Forbes*

Received 00th January 20xx,
Accepted 00th January 20xx

DOI: 10.1039/x0xx00000x

www.rsc.org/

Physical properties of actinyl materials are influenced by the presence of oxo functional groups. Herein, we report large thermal expansion coefficients for a uranyl metal organic nanotube that switch from positive to negative upon dehydration. Different behaviour is observed in the neptunyl system due to variations in the oxo interactions.

Metal organic materials represent an expansive family of compounds that have traditionally been developed for high sorption capabilities, but a handful of these compounds display unusual thermal expansion behaviour.[1-3] Most materials exhibit an increase in volume upon heating, termed positive thermal expansion (PTE). The coefficient of thermal expansion (CTE) denoted as 'α' represents the change in the lattice parameters (or volume) across a thermal gradient. Typical inorganic materials have α values ranging from 0-20 MK^{-1}, whereas metal organic materials have values that can reach up to +653.2 MK^{-1} (M = 10^{-6}).[2] Contraction upon heating, or negative thermal expansion (NTE), is quite rare for inorganic materials, with oxides like ZrW_2O_8 being the most well-studied compounds.[4-7] Within metal organic materials, negative thermal expansion is observed more often and usually it occurs along a single crystallographic axis (97% of reported cases).[2] Negative α values for metal organic compounds range between -17 and -148 MK^{-1}, but the overall (volumetric) thermal expansion generally remains positive due to expansion in the other crystallographic directions.[2]

Understanding the structural drivers that lead to anomalous thermal expansion behaviour is important for the development of these materials, particularly in the case of rare NTE compounds. PTE is typically associated with the asymmetry of the equilibrium bond length curve, whereas mechanisms that lead to NTE include structural transformations, transverse vibrational modes, or spin cross-over effects.[6] Within metal organic materials, structural transformations associated with flexibility of the ligands are often linked to the anomalous behaviour.[2] More specifically, changes in the intramolecular angles and bond distances can lead to conformational changes or rearrangements of crystalline packing and impact overall lattice behaviour. The presence of guest molecules can also influence the thermal expansion properties, but this mechanism is less clear. For example, Wei et al.[8] and Goodwin et al.[9] reported variations in CTEs upon inclusion of different guest molecules, but the diffuse nature of the encapsulated molecules did not provide sufficient structural information to fully explain the thermal behaviour.[9] Only Zhou et al. provided some information on how the rearrangements of guest molecules within a porous material influenced the thermal expansion properties (*vide infra*).[10]

Our research group focuses on high-valent (V, VI) actinide metal organic materials and the unique structural features that result in new chemical and physical properties. Many of the early actinide elements with oxidation states of V or VI form two strong bonds with O atoms to create a nearly linear dioxo cation $(AnO_2)^{+/2+}$. In the case of uranyl $(U(VI)O_2)^{2+}$, the oxo groups are essentially passivated and exhibit limited interactions with the surroundings.[11] The structural influence of the uranyl moiety on metal organic materials has been described by other groups, including but not limited to Cahill,[12] Thuery and Harrowfield,[13] and Loiseau.[14] These groups report a propensity for lower dimensional materials and weak intermolecular interactions with the oxo group. Pentavalent actinyl cations, such as $Np(V)O_2^+$, are less studied due to difficulties in working with ^{237}Np, but the stronger basicity of the neptunyl oxo leads to a higher proportion of 3-D structures and stronger interactions to nearby molecules.[15] The inequivalent oxo character will likely influence the chemical and physical properties (including thermal expansion behaviour) of the resulting compounds; thus, we focus on the structure-function relationships for these materials.

[a] *Department of Chemistry, University of Iowa, Iowa City, IA 52242 Corresponding author: tori-forbes@uiowa.edu*

Electronic Supplementary Information (ESI) available: [details of any supplementary information available should be included here]. See DOI: 10.1039/x0xx00000x

The current study explores the thermal expansion behaviour of a uranyl iminodiacetate compound (UMON) that contains ordered water molecules as nanoconfined guests within a 1-D channel.[16] We report colossal negative thermal expansion behaviour for dehydrated UMON and contrast that with the direct interactions between the uranyl oxo groups and confined water molecules within the hydrated form. We also describe our efforts within the related Np iminodiacetate system for $Np(VI)O_2^{2+}$ and $Np(V)O_2^{+}$ cations and highlight the impacts of redox activity and differences in oxo interactions on the final products. Lastly, we report the first thermal expansion coefficients of a Np(V) compound and again correlate the behaviour to interactions with the neptunyl oxo groups.

We synthesized UMON crystals according to a previously published procedure.[16] Variable temperature single-crystal X-ray diffraction data were collected on three different UMON crystals, from three different synthetic batches for both the hydrated and dehydrated specimens. Neptunyl compounds were formed by combining similar components from the UMON synthesis to a Np(V) or Np(VI) stock solution. Additional information regarding synthetic details and structural characterization parameters are provided in the SI.

Hydrated and dehydrated forms of the UMON material crystallize in the trigonal space group *P*-3 and the asymmetric unit contains the uranyl cation, two iminodiacetate ligands, one-half of a piperazinium cation, and two lattice water molecules. The uranyl cation is coordinated by one of the iminodiacetate ligands in a tridentate fashion and the second molecule serves as a monodentate linker, forming a pentagonal bipyramidal geometry about the metal centre. Six uranyl units are connected to form macrocyclic segments that stack into a nanotubular assembly with an overall pore diameter of 12 Å (Fig. 1a). Two crystallographically unique water molecules (OW1 and OW2) are located within the channels of the hydrated material. These guest water molecules self-assemble into a 1-D "ice-like" structure through an extensive H-bonding network. These guests can be removed by heating to 310K and the channel does not collapse upon dehydration (Fig. 1b). Rehydration can occur upon exposure to water vapour, with complete hydration occurring within 20 minutes.

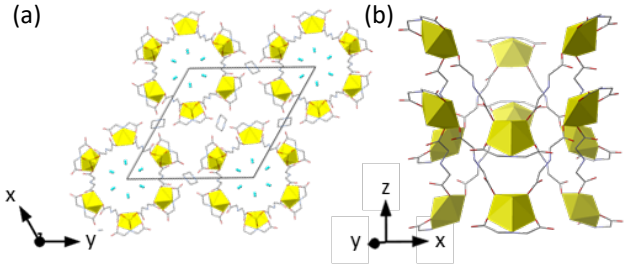

Figure 1. (a) Hydrated and (b) dehydrated UMON structure. The U is depicted as yellow polyhedra and the iminodiacetate ligand is shown as a wire model. The water molecules are illustrated using teal spheres and the H atoms are removed for clarity.

Unit cell parameters for the UMON samples collected at 100K were comparable to the values previously reported by Unruh et al.[16] The hydrated crystal possessed average unit cell dimensions of a_{av} = 22.2363(44) and c_{av} = 6.613(10) Å, whereas the a_{av} and c_{av} parameters for the dehydrated sample were 22.692(34) and 6.4956(29) Å, respectively. At 100K, the dehydrated unit cell volume is ~65 Å^3 larger than the hydrated material. This contraction in the volume upon hydration is quite unusual because typically the addition of solvent molecules to porous metal organic materials results in an increase in the volume.[8]

A small positive change in the unit cell volume occurs in both the dehydrated and hydrated UMON samples as the temperature increases from 100-200K (ΔV_{av} = +13 and +35 Å^3 respectively) and then significant deviations occur from 200-260 K. After 200K, the hydrated sample continues to exhibit PTE, albeit at a smaller rate (ΔV_{av} = +7 Å^3). However, the dehydrated compound exhibits a sudden decrease in volume that leads to NTE behaviour in this region (ΔV_{av} = -15 Å^3).

As one would imagine from the changing volumes, the variations in the principal strain axes are not uniform and the UMON material exhibits thermal expansion that varies with hydration state. For the hydrated material, the *c* parameter initially remains relatively constant and then decreases 0.05 Å (0.7%) in the region from 200-260K. The *a* parameter exhibits the opposite behaviour with a slight increase between 100-200 K followed by a more substantial gain at higher temperatures. Turning to the dehydrated sample, the *c* parameter remains relatively constant across the entire temperature regime. The *a* parameter for the dehydrated material also remains constant from 100-200K and then decreases between 200-260K. Overall the dehydrated sample displays relatively isotropic thermal behaviour, but the hydrated sample responds to thermal changes anisotropically.

From these studies, we can calculate α values for the *a* and *c* directions (α_a and α_c) and the volumetric expansion coefficient (α_V) for both the hydrated and dehydrated samples between 200 and 260K (Table 1). For the hydrated sample, a negative coefficient of thermal expansion is observed in the *c* direction with a value of $\alpha_{X1} = \alpha_c$ = -112(3) MK^{-1}. Scrutinizing the *a* (=*b*) lattice parameter, the expansion behaviour is best described as moderate positive thermal expansion, with principal axes $\alpha_a \cong \alpha_{X2} = \alpha_{X3}$ = 83(15) MK^{-1}. For the dehydrated material the thermal expansion coefficients are calculated at -47(11), -51(11), and -13(3) for $\alpha_a \cong \alpha_{X1}$, $\alpha_a \cong \alpha_{X2}$ and $\alpha_c = \alpha_{X3}$, respectively. The combination of the small and moderate NTE along the principal axes results in a colossal volumetric contraction with a coefficient of α_v = -162(35)MK^{-1}. This result is noteworthy not only because of its negative value, but also because contraction occurs along each principle axis. As stated earlier, NTE behaviour in metal organic materials rarely occurs along all three axes. The UMON material and a very recent report of an In MOF[17] are the only reported metal organic materials that exhibit NTE along all three principal axes.

The mechanism for the NTE behaviour in the dehydrated UMON material can be traced to the flexible IDA linker that exhibits a subtle conformational change along the temperature gradient. Specifically, the C-N-C bond angle decreases by ~0.5° from 200-260K compared to the analogous angle associated with the chelating IDA molecule, which remains relatively constant. This C-N-C bond angle is canted ~65° from the (001)

plane (Fig. 2, S7), thus any movement will affect all three principal axes and create a 'lattice-fence' effect. Zhou et al.[18] also described this lattice-fence effect when they reported NTE in MCF-34, a Mn(II) framework material that contains 1-D channels. In the MCF-34 material, a smaller L-Mn-L angle decreased the *c* axis, but the canted angle of the ligand also caused a lengthening of the *a* and *b* axes.[18] The cooperative effects in MCF-34 results in an overall positive thermal expansion, which is different from what is observed within the dehydrated UMON material.

Table 1. Principal coefficients of thermal expansion for hydrated and dehydrated UMON and corresponding approximate crystallographic direction calculated with PASCal.[19]

	Axis	α (MK^{-1})	Crystallographic direction
Hydrated UMON	X_1	-112(3)	0 0 1
	X_2	83(15)	-3 1 0
	X_3	83(15)	3 4 0
	V	142(42)	
Dehydrated UMON	X_1	-47(11)	-3 1 0
	X_2	-51(11)	3 4 0
	X_3	-13(3)	0 0 1
	V	-162(35)	

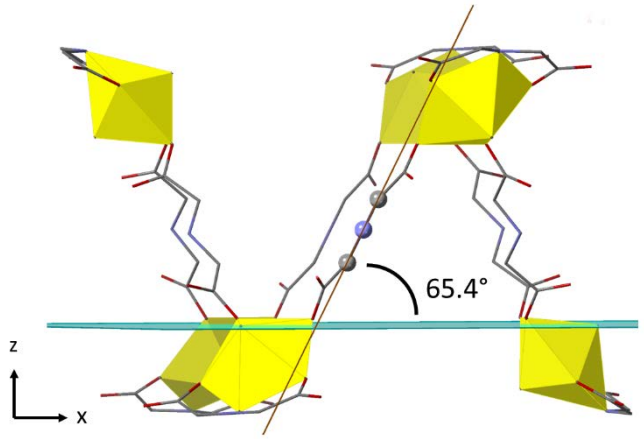

Figure 2. Changes in the C-N-C bond angle within the iminodiacetate linker molecule for the dehydrated nanotube. U(VI) is represented by yellow polyhedra and the iminodiacetate molecules are depicted as wire representations. Cyan plane represents (001) crystallographic plane.

Within the hydrated UMON material, we observe that the guest molecules alter the thermal expansion behaviour, but in a different manner than prior literature reports. The hydrated framework displays stronger NTE along the *c*-axis and PTE along the *a* direction. Previous studies by Wei et al.[8] and Zhou et al.[18], observed differing magnitudes for the α parameter, but not a switch between positive and negative expansion behaviour based upon incorporation of guest molecules. Goodwin et al.[9] reported a similar phenomenon in $ZnPt(CN)_6$ X H_2O, where the α_a parameter changed from +1.82(15) MK^{-1} for the hydrated form (X = 2) to -3.2(9) MK^{-1} for the dehydrated (X = 0) material. In the hydrated UMON material, the *a* axis is now positive and that changes the overall volumetric thermal expansion behaviour from negative to positive upon hydration. The magnitude of the change is also significant because the α_V varies by 300 MK^{-1} (-162 to +142 MK^{-1}) upon hydration.

We attribute the difference in the α_a behaviour to a repulsive stabilization effect between a uranyl oxo and the water molecules of the hydrated framework (Fig. 3, S8). Gagliardi and others have well established that the uranyl oxo will not engage in hydrogen bonding with water molecules in bulk solvent,[20, 21] but there is no literature precedent for confined water. The well-ordered water array of our UMON provides an excellent opportunity to further explore this interaction. The high-quality X-ray diffraction data allows for the location of H atoms within the difference Fourier map. These H-atoms are engaged in hydrogen bonding between water molecules, both within the hexameric water unit and to water units above and below. The O atoms of the water molecules are pointed towards the uranyl oxo at an interatomic distance ~3.4 Å. Introductory chemistry textbooks describe the water molecule by a sp^3 electron domain geometry with two bonds to H atoms and two lone pairs, resulting in the well-known bent molecular geometry. Ab initio calculations suggest that a better model includes a diffuse area of electron density within the region where the lone pairs are nominally located.[22] The radial distribution of the electron density is not spherical and slight indentations exist opposite the putative electron pairs. Neutron diffraction experiments found that interactions between the "lone pairs" of neighbouring water molecules resulted in an interatomic O-O distance of a ~3.4 Å.[23] This distance and geometry is consistent with our observations of the arrangement between nanoconfined water molecules and the uranyl oxo group within the hydrated UMON material.

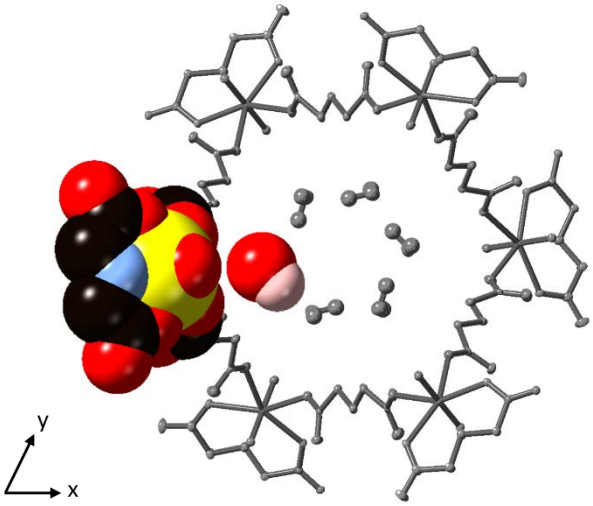

Figure 3. Repulsive interactions between the O atom in the OW1 water and the O atom of the uranyl oxo are represented through a shape filling representation. The radii for the spheres are the van der Waal radii. U, O, N, C, and H are represented by yellow, red, light blue, black, and pink spheres, respectively.

The larger negative thermal expansion value (α_c) for the hydrated UMON material is further explained by the formation of an extensive H-bonding network among the confined water molecules. As the temperature is decreased, the confined water molecules become more ordered (as evidenced by smaller ellipsoids). The molecules occupy more space, which leads to subsequent NTE along the channel. Birkedal et al. also reported this phenomenon in their dipeptide nanotube that contained confined water.[24] Furthermore, because weak H-bonds exist

between the OW2 molecule and UMON framework (carboxylate O atoms D…A =3.2 Å) the cooperative effects of the enhanced water ordering likely work to shift the uranyl macrocycles further away, leading to NTE in the direction normal to the (001) plane.

Attempts to synthesize a Np MON material were unsuccessful, but provide additional insight into the impact of the oxo bond interactions. Redox activity hampered the ability to form Np(VI) compounds, as reduction to Np(V) was noted in this system. Np(VI) is not the dominant oxidation state under these experimental conditions and reduction of the Np in the presence of organic ligands has been reported in the literature.[25] Reactions with Np(V) resulted in the formation of two novel compounds: $(Np(V)O_2(C_4NO_4H_6))$ and the first isolated example of a $Np(V)O_2$ tetrachloride unit, $(N_2C_4H_{12})_2[Np(V)O_2Cl_4]Cl$) (Tables S2-S4; Fig. S11-14). Within $(Np(V)O_2(C_4NO_4H_6)$, the iminodiacetate ligand does not chelate the NpO_2^+ unit and instead serves as linkers to create infinite sheets. For $(N_2C_4H_{12})_2[Np(V)O_2Cl_4]Cl)$, the iminodiacetate molecule is completely absent from the structure and four Cl anions coordinate to the NpO_2^+ cation. Piperazinium cations are present in the structure to charge balance the $[NpO_2Cl_4]^{-3}$ units. In both compounds, there is significant H-bonding to the neptunyl oxo groups, either through the doubly protonated amine group located in the centre of a neighbouring iminodiacetate molecule (D…A = 2.77 Å) or to the charge balancing piperazinium cations (D…A = 2.74 – 2.95 Å). This strong H-bonding interaction may hinder the formation of porous metal organic materials within the Np(V) system.

Strong H-bonding interactions with the neptunyl oxo also influence the expansion behaviour of $(N_2C_4H_{12})_2[Np(V)O_2Cl_4]Cl)$. Crystallinity of $(Np(V)O_2(C_4NO_4H_6))$ was of lower quality, so we chose to focus solely on the $[Np(V)O_2Cl_4]$ coordination compound. Temperature dependent XRD data was collected for $(N_2C_4H_{12})_2[Np(V)O_2Cl_4]Cl)$ from 200 to 260 K (see SI). Overall, the material displayed the expected PTE (α_V = 80(5) MK^{-1}) but exhibits anisotropic behaviour. The α_b (+30(3) MK^{-1}) and α_c (+49(3) MK^{-1}) coefficients are positive, but the α_a is slightly negative (-2.8(9) MK^{-1}). This is significant because the H-bond between the neptunyl oxo and the piperazinium cations lies within this crystallographic axis, demonstrating the importance of this attractive force in creating the NTE behaviour.

This study highlights the ability of the oxo functional group to influence the physical properties of actinide metal organic materials. The PTE behaviour of the hydrated UMON material can be explained by the repulsion between the uranyl oxo group and the nanoconfined water molecules. Increased basicity of the oxo group for the $(Np(V)O_2)^+$ cation results in attractive H-bonding forces and leading to NTE along that axis. Future studies will continue to explore the interaction of actinide materials with nanoconfined water molecules and the impact of the actinyl oxo group on the chemical and physical properties of metal organic coordination compounds.

Conflicts of interest

There are no conflicts of interest to declare.

Acknowledgements

MKP and work associated with the thermal expansion of the UMON material is supported by the NSF Division of Material Research Solid-State Chemistry program (DMR1252831). MMP, MMJ, MCB, and experiments with Np-237 are supported by the DOE Heavy Elements Program (DE-SC0013980).

Notes and references

1. S. Seth and A. J. Matzger, *Cryst. Growth Des.*, 2017, **17**, 4043-4048.
2. Z. Liu, Q. Gao, J. Chen, J. Deng, K. Lin and X. Xing, *Chem Commun*, 2018, **54**, 5164-5176.
3. C. H. Hendon, A. J. Rieth, M. D. Korzyński and M. Dincă, *ACS Cent. Sc.*, 2017, **3**, 554-563.
4. C. Martinek and F. Hummel, *J. Am. Ceram. Soc.*, 1968, **51**, 227-228.
5. T. A. Mary, J. S. O. Evans, T. Vogt and A. W. Sleight, *Science*, 1996, **272**, 90-92.
6. W. Miller, C. W. Smith, D. S. Mackenzie and K. E. Evans, *J. Mater. Sci.*, 2009, **44**, 5441-5451.
7. C. Lind, *Mater.*, 2012, **5**, 1125.
8. Y. S. Wei, K. J. Chen, P. Q. Liao, B. Y. Zhu, R. B. Lin, H. L. Zhou, B. Y. Wang, W. Xue, J. P. Zhang and X. M. Chen, *Chem. Sci.*, 2013, **4**, 1539-1546.
9. A. L. Goodwin, K. W. Chapman and C. J. Kepert, *J. Am. Chem. Soc.*, 2005, **127**, 17980-17981.
10. H.-L. Zhou, R.-B. Lin, C.-T. He, Y.-B. Zhang, N. Feng, Q. Wang, F. Deng, J.-P. Zhang and X.-M. Chen, *Nature Commun*, 2013, **4**, 2534.
11. P. C. Burns, *The Can. Mineral*, 2005, **43**, 1839-1894.
12. M. B. Andrews and C. L. Cahill, *Chem. Rev.*, 2013, **113**, 1121-1136.
13. P. Thuery and J. Harrowfield, *Dalton Trans.*, 2017, **46**, 13660-13667.
14. T. Loiseau, I. Mihalcea, N. Henry and C. Volkringer, *Coord. Chem. Rev.*, 2014, **266**, 69-109.
15. J. J. Katz, L. R. Morss, N. M. Edelstein and J. Fuger, *The Chemistry of the Actinide and Transactinide Elements (Set Vol.1-6)*, Springer Netherlands, 2010.
16. D. K. Unruh, K. Gojdas, A. Libo and T. Z. Forbes, *J. Am. Chem. Soc.*, 2013, **135**, 7398-7401.
17. Z. N. Liu, Q. Li, H. Zhu, K. Lin, J. X. Deng, J. Chen and X. R. Xing, *Chem. Commun.*, 2018, **54**, 5712-5715.
18. H. L. Zhou, M. Li, D. Li, J. P. Zhang and X. M. Chen, *Sci. China-Chem.*, 2014, **57**, 365-370.
19. M. J. Cliffe and A. L. Goodwin, *J. Appl. Cryst.*, 2012, **45**, 1321-1329.
20. D. Hagberg, G. Karlström, B. O. Roos and L. Gagliardi, *J. Am. Chem. Soc.*, 2005, **127**, 14250-14256.
21. P. Miró, B. Vlaisavljevich, A. L. Dzubak, S. Hu, P. C. Burns, C. J. Cramer, R. Spezia and L. Gagliardi, *J .Phys. Chem. C*, 2014, **118**, 24730-24740.
22. M. Laing, *J.Chem. Ed.*, 1987, **64**, 124.
23. I. Pethes and L. Pusztai, *J. Molec Liq.*, 2015, **212**, 111-116.
24. H. Birkedal, D. Schwarzenbach and P. Pattison, *Angew. Chem. Int. Ed.*, 2002, **41**, 754-756.
25. D. T. Reed, D. G. Wygmans, S. B. Aase and J. E. Banaszak, *Radiochimica Acta*, 1998, **82**, 109-114.